Available online at www.sciencedirect.com

ScienceDirect

Procedia CIRP 00 (2022) 000–000

www.elsevier.com/locate/procedia

12th CIRP Conference on Photonic Technologies [LANE 2022], 4-8 September 2022, Fürth, Germany

Strain-based investigation on solidification crack susceptibility of 6005 aluminium using adjustable ring mode (ARM) laser welding

Venkat Vivek Pamarthi[a], Tianzhu Sun[a], Abhishek Das[b], Pasquale Franciosa[a]

[a]*WMG, University of Warwick, Coventry, United Kingdom*
[b]*Mechanical Engineering department, Indian Institute of Technology, Delhi, India*

* Corresponding author. Tel.: +44 7393077458; *E-mail address:* venkat-vivek.pamarthi@warwick.ac.uk

Abstract

Solidification cracks are among the most deteriorating defects observed in Remote Laser Welding (RLW) of 6xxx aluminium alloys. This research has been designed to study the solidification crack susceptibility during RLW of AA6005 alloy using Adjustable Ring mode (ARM) laser technology. The experimental setup included a high-speed camera on the self-restraint test rig, and the strains near the root of the solidification front were identified with a Finite Element based Digital Image Correlation (DIC) technique. This DIC technique allows the precise measurement of displacements and evaluates the strains at the root of the melt pool, and further correlates the critical strains formed near the root with the power ratios of the core and ring beam. A process window relating the total laser power and the power ratio to the cracking susceptibility was identified. Although a linear dependency exists between power ratio and weld penetration depth, the same does not apply to the crack sensitivity since a parabola-like relationship was observed. Findings suggested that the transition from coarse to fine equiaxed grains at increasing power ratios reduces the crack sensitivity to the threshold power ratio of 1.5. It reveals that the cracking susceptibility is determined by the combined effect of the grain refinement (predominant at power ratios below 1.5) and the permeability in the fusion zone (predominant at power ratios above 1.5).

Keywords: 6005 Aluminium Alloys, Solidification Cracking, Adjustable Ring Mode Laser, Digital Image Correlation, Transverse Strain, Power Ratio.

1. Introduction

In recent years, a constant urge toward net-zero emissions transport and reduction of fuel consumption has developed the need to use lightweight materials [1]. Given the excellent strength-to-weight ratio, corrosion resistance and recycling capability, aluminium alloys are being adopted to reciprocate the advantages of high-strength steel structures in Electric Vehicle (EV) manufacturing [2] and body construction. A recent report [3] has indicated that the use of 6xxx series aluminium alloys (both extrusions and sheets) will rapidly increase from the current level of approx. 20 kg used in internal combustion engine vehicles to up to 250 kg for EVs. Together with the selection of materials, the joining process plays a crucial role to fulfil various manufacturing requirements such as cost, functional performance and production volume. Laser welding has attracted interest in recent years due to its low heat input and high energy density, high welding speed, low thermal distortion and enhanced flexibility [2].

Solidification cracking is certainly one of the most critical and commonly encountered defects during laser welding of 6xxx series (Al-Mg-Si) alloys [4]. It has attracted considerable attention from industrial practitioners and researchers [5]. It involves a complex interaction in the fusion zone and the solidification properties of the alloy. The generalized cracking theory states that a crack initiates in the last solidification phase, also called the mushy zone, where the continuous molten films separate the growing dendrites, and the local tensile strains overtake its strength to form a crack. According to recent studies on solidification cracking, the strains and critical strain rate near the termination point of the solidification front are the main variables that decide the crack sensitivity [6]. The strain-based criteria developed by

Rappaz, Drezet and Gremaud (RDG) [7] have shown the significance of critical strain rate measurements in understanding solidification cracking. It was seen from a modified RDG model that excessive refinement in the grain size will also affect the mushy zone's permeability and increase the crack susceptibility [8].

The control of the cracking susceptibility has seen the implementation of various methods: (1) the modification to the chemical composition of the molten pool using filler wires (either 4xxx or 5xxx aluminium wires) is currently the best practice in industry (tactile laser welding); (2) the grain refinement by addition of nucleators such as titanium [2]; and, (3) the grain refinement by controlled heat input via a combination of power modulation, beam oscillation and beam shaping [9]. The beam shaping technology uses a multi-beam and multi-focal approach and holds the promise to control the cooling rates and thermal gradients in and around the molten pool. It mainly consists of two types: (1) tandem beam made of two (or multiple) laser beams either arranged parallel or side by side in the welding direction [10]. Xie et al. [2] studied the centreline cracking in both single and tandem dual-beam during welds of 1045 steel plates and concluded that the crack susceptibility using a tandem beam is comparatively less than the single beam; (2) co-axial dual laser beam (also known as Adjustable Ring Mode (ARM)) that provides independent control of power distribution in the inner core laser beam and outer ring-shaped laser beam. The inner core promotes the generation of the keyhole, while the ring-shaped laser beam allows controlling the distribution of thermal profiles in and around the molten pool. Research has confirmed a positive effect of the ARM laser on keyhole stabilization [11], [12]. Only a few attempts with scattered results have been made to study the impact of beam shaping on crack susceptibility. Minjung et al. [13] used the ARM technology to weld AA 6016 alloy and observed that the power distribution enhanced the grain morphology but could not find evidence of reduction of crack susceptibility.

This paper aims at studying the susceptibility of solidification cracking during RLW of AA6005 alloy using Adjustable Ring mode (ARM) laser technology. This is achieved by in-process monitoring the crack at different power ratios (power of the inner core divided by the power of the outer ring) using a high-speed camera and a self-restraint test rig. An ad-hoc Finite element (FE) based Digital Image Correlation technique (DIC) was then implemented to measure the transverse strains developed near the crack initiation. Finally, the strains were measured near the crack tip (the root of the solidification front) and analyzed to interpret the effect of different power ratios.

2. Materials and methods

2.1. Experimental Setup

The tests were carried out using a self-loaded hot cracking setup with an overlap joint configuration. The material used was AA 6005 sheets, 3 mm thickness and chemical composition given in Table 1. Samples were machined into the size of 100 mm (length) × 50 mm (width) before welding.

Generally, a solidification cracking test setup must be externally or internally loaded to investigate the strain conditions during cracking [14]. The self-loaded cracking test setup generates local strains based on the weld positions from the free edge as shown in Fig 1 and therefore allows to visualize the loading conditions acting on the weld metal[15]. All the welded seams were performed at 10 mm from the free edge in the overlap joint configuration, as shown in Fig 1.

Table 1. Chemical composition (in wt.- %) of the investigated material.

Mn	Fe	Mg	Si	Cu	Mg+Cr	Zn	Others	Al
0.5	0.35	0.4	0.5	0.1	0.12	0.1	0.05	Bal.

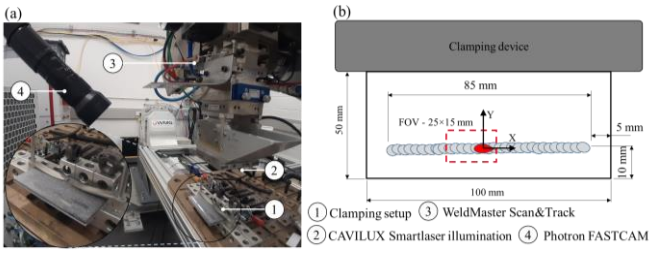

Fig 1. (a) welding equipment; (b) representation of the self-restraint test rig.

The specimens were welded by the Coherent CW multi-mode fibre laser HighLight FL-ARM 10000. The ARM beam was delivered through the WeldMaster Scan&Track remote welding head (YW52 Precitec GmbH, Germany). All experiments were performed without shielding gas and without filler wire. Details of the welding setup are in Table 2.

Table 2. Technical specifications of the welding setup.

FL-ARM 10000 & Weld Master	Units	Core	Ring
Maximum output power	W	5000	5000
Optical fibre diameter	µm	100	290
Spot diameter at the focus	µm	200	580
Emission wavelength	nm	1080	
Rayleigh length	mm	5.3	
Focusing length	mm	300	
Collimating length	mm	150	

A Photron FASTCAM NOVA S6 and CAVILUX Smart laser illumination (808 nm with exposure of 20 µs and fps of 20000) were used to observe the crack formation, with a static field of view (FOV) of 25×15 mm^2, centered at the middle of the weld. The camera's frame rate was 12000 fps with a resolution of 896 × 320 pixels. In order to get the strains from either side of the fusion zone, in addition to the laser illumination, a speckled paint was used. It consisted of Kontakt Graphite aerosol as the dark background and Combat Boron nitride aerosol as the white stochastic pattern that can withstand high temperatures.

A dye penetrant test was implemented to confirm the crack formation on the welded specimens. A ROCL leak and flaw detector spray was used with a developer time of 5 seconds to inspect the cracks visually. For microstructural analysis, cross-sections of each sample were cut, hot mounted and polished using the SIC abrasive paper, diamond suspension and the colloidal silica slurry. The weld morphology was analyzed by Nikon Eclipse LV150N optical microscope. Grain morphology of the welded cross-section was analyzed by JEOL 7800F, a field emission scanning electron microscope equipped with an Electron backscattered diffraction (EBSD) system with a step size of 3 µm. The EBSD acquisition and processing were performed on Aztec

HKL and AztecCrystal software.

2.2 Definition of process parameters

Two parameters, namely the power ratio (power core divided by power ring), *r*, and the total power (cumulated between core and ring), *P*, were changed to analyze the effect of ARM beam on crack sensitivity. The laser beam was delivered with a sinusoidal beam oscillation in the Y-axis and was focused 2 mm below the top surface. Detailed parameters are in Table 3. Power ratios of 0.36 and 2.5 for *P*=7000 W were not investigated since they fall outside the maximum power of the core and ring beam. Representative distributions of power density at different power ratios are shown in Fig 2.

Table 3. Definition of process parameters.

Total power, *P*	**Power ratio, *r***
5000 W 6000 W	0.36; 0.67; 1; 1.5; 2; 2.5
7000 W	0.67; 1; 1.5; 2
Fixed parameters	
Welding speed (mm/s)	50
Oscillation amplitude (mm)	2.5
Oscillation Frequency (Hz)	100
Focal offset (mm)	-2 (below the top surface)

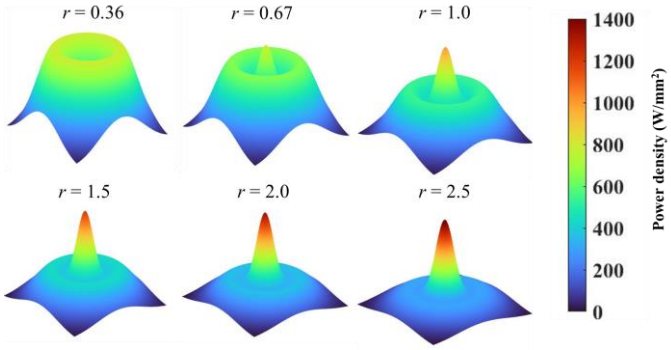

Fig 2. Representative distributions of power density for variable power ratios (for a total power of 5000 W).

As the welding speed was kept constant, the total welding time was 1.7 seconds for every specimen. The high-speed camera images were recorded for 0.6125 seconds.

2.3 Digital image correlation and strain measurement

Despite strain gauges and induction types [16] being the most established sensors to measure strains, they can only be used outside the fusion zone. They cannot be used near the immediate vicinity of the molten pool because of the high-temperature conditions. In recent studies, contactless measurement techniques, such as image correlation techniques, have been successfully implemented to measure strains around the molten pool. Hagenlocher et al. [17] used Digital Image Correlation (DIC) technique with the GOM software to measure the critical strains produced on either side of the weld. Since this paper aims at investigating the strains directly in the weld zone, the approach in [17] cannot be directly used in this paper due to the disturbances generated by the plume emissions. Therefore, the Finite Element (FE)-based DIC technique with an adaptive haze removal algorithm and un-sharp masking for pre-processing the data has been implemented to reduce the plumes effect and disturbances generated during the welding process. The FE-based correlation algorithm, originally developed by Yang J. et al. [18], was adapted in this study and coded in MATLAB. The reference image and the region of interest (ROI) were taken after the melt pool, as shown in Fig. 3(a). The deformation for the next images was calculated by correlation with this reference image.

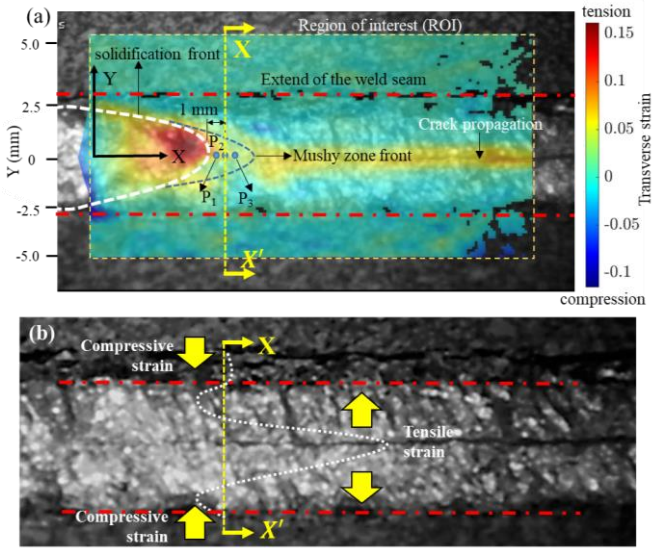

Fig 3. (a) transverse strains (ε_{yy}) near the crack initiation and near the end of the melt pool observed using the FE-based DIC technique; (b) schematic representation of transverse (both compressive and tensile) strains along the X-X' section.

The transverse strains, ε_{yy} (acting along the Y-axis (Fig. 3(a)), were calculated in three locations, P_1, P_2 and P_3, near the root of the solidification front, approximately at the end of the mushy zone (the 3 points were equally spaced at 0.5 mm). The distribution of transverse strains was also calculated along the transversal section, marked X-X'. Fig. 3(b) shows a schematic representation of the formation of transverse strains near the crack initiation: *compressive strains* which are formed on either side of the crack due to shrinkage stresses; *tensile strains* in the middle of the seam due to large transverse tensile strains during cracking [5].

3. Results and discussion

3.1 Microstructural characterization

The weld profile of each welding set is shown in Fig. 4(a), and the results of dye penetrant tests are in Fig 4(c). It is observed that as the power ratio increased from 0.36 to 2.5, at all power levels, the penetration depth increased due to the increase in power density. A linear correlation between penetration depth and power ratio was observed.

Further, as the power level increased from 5000 W to 7000 W, there is an evident formation of a centreline crack as shown in Fig. 4(a). This result corroborates the facts that an increase in laser power increases the lateral heat flow inside the material, hence, increasing the crack sensitivity .

3.2 Distribution of transverse strains (X-X' section)

Fig. 5 shows the distribution of the transverse strains, measured along the X-X' section. Results are as follows:

- *P*=5000 W and *P*=6000 W: at a power ratio of 0.36, high tensile strains near the fusion zone and centreline cracks were observed. As the power ratio increases and reaches a threshold of 1.5, the compressive strains dominate in the fusion zone, and no centreline cracks were observed. Further increasing to 2.5 leads to transverse cracks, indicating an increase in crack sensitivity but no sign of centreline cracks.
- *P*=7000W: the transverse strains for the lower power ratios were higher than those observed at *P*=5000W and *P*=6000W, indicating the formation of both centreline and transverse cracks in the fusion zone.

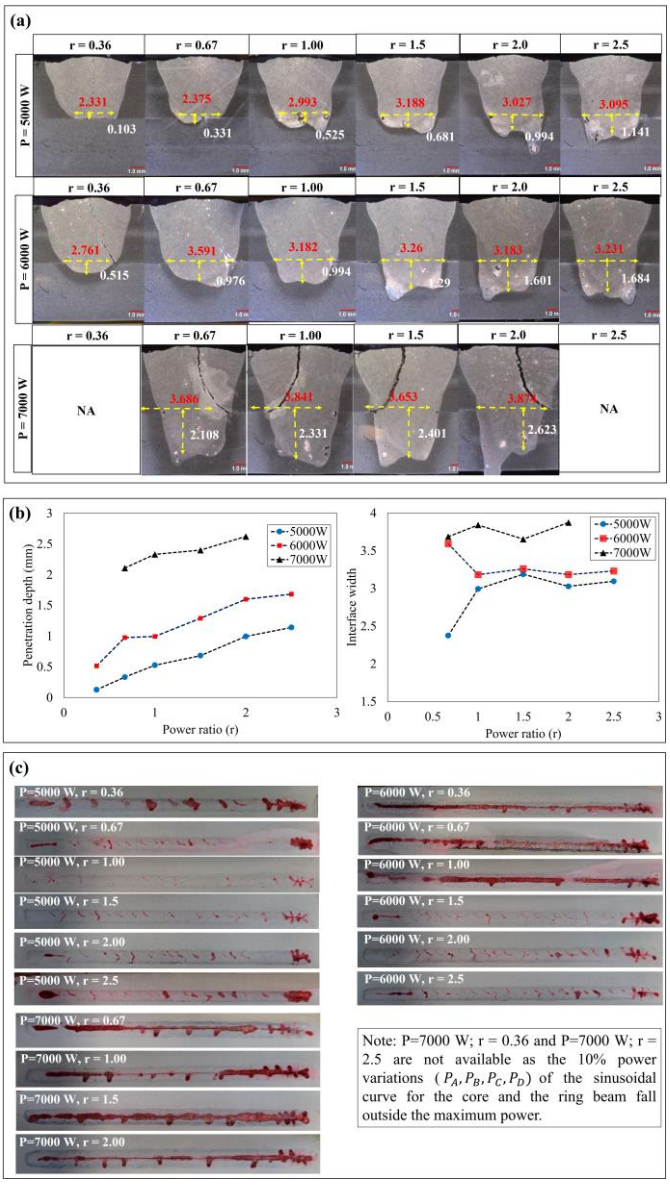

Fig 4.(a) optical micrographs; (b) measurement of weld penetration depth and interface width; (c) dye penetrant test results of the sample - both centreline and transverse cracks are observed.

3.3 Effect of power ratio on crack susceptibility

Fig. 6(a) shows the peak transverse strains observed near the root of the solidification front (averaged values across the 3 locations, P_1, P_2 and P_3) against the power ratios. The variability observed with the power ratio has been statistically tested with ANOVA, and the results confirmed the significance (p-value below 5%).

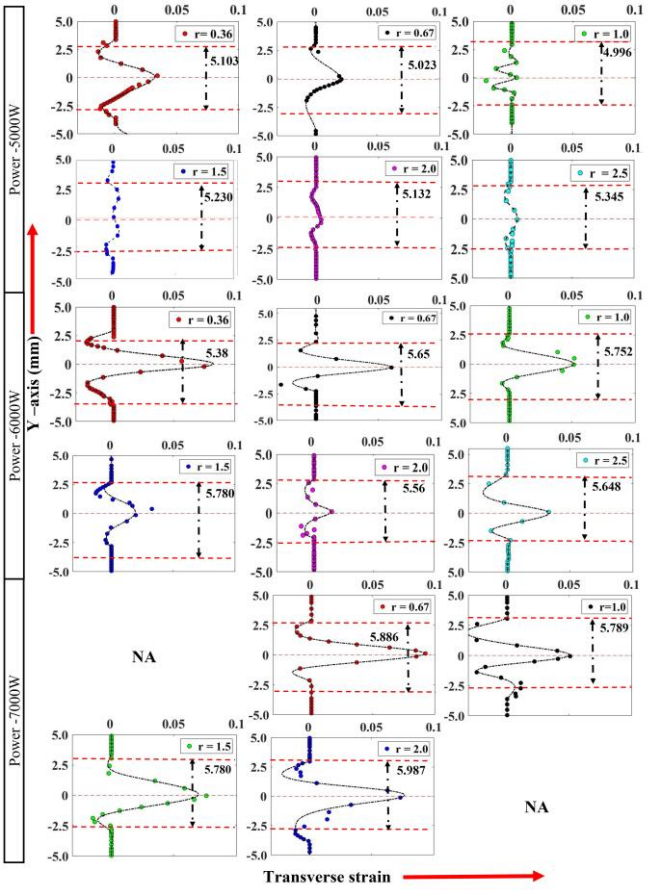

Fig 5. Distribution of the transverse strains (measured along the X-X' section) near the end of the solidification front at different power levels and ratios. The dotted lines represent the extend of the weld seam.

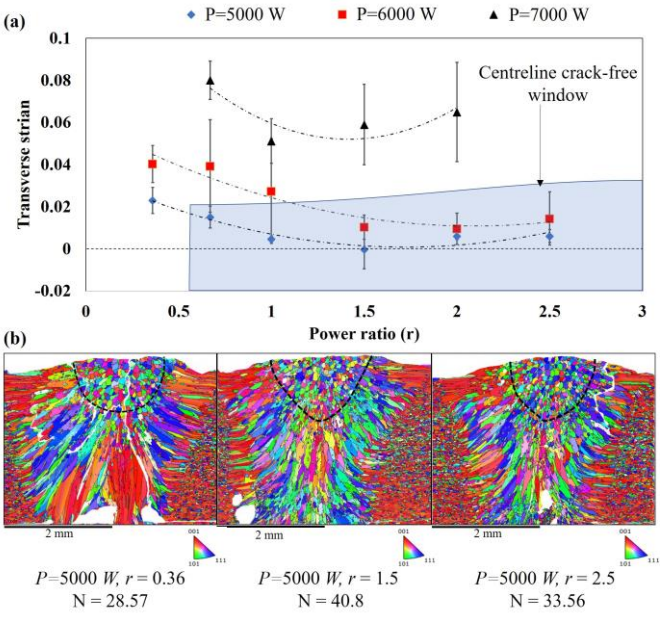

Fig 6.(a) peak transverse strains observed near the root of the solidification front (averaged values across the 3 locations P_1, P_2 and P_3); (b) EBSD map for P=5000 W at power ratio of 0.36, 1.5 and 2.5.

It is worth noting that although a linear dependency exists between power ratio and weld penetration depth (Fig. 4(b)), the same does not apply for the crack sensitivity (Fig. 6(a)

shows a parabola-like relationship). This confirms a strong and complex dependency between power level and power ratio.

To discuss the results in Fig. 6(a), the temperature gradient, G, and the solidification rate, R, have been introduced. The multiplication of G and R gives the cooling rate observed near the solid-liquid interface, and the ratio of G and R determines the morphology of the solidification structure (planar, cellular, columnar and equiaxed structure).

Many researchers have studied the effect of G and R on the fusion zone [5], [8]. A schematic plot is shown in Fig. 7, adapted from the original Kurz and Fisher's diagram [19]. Since in this paper the beam oscillation parameters (amplitude and frequency) are kept constant, the grain size (related to GxR) and morphology (related to G/R) only depend upon the varied power distributions of the ARM beam.

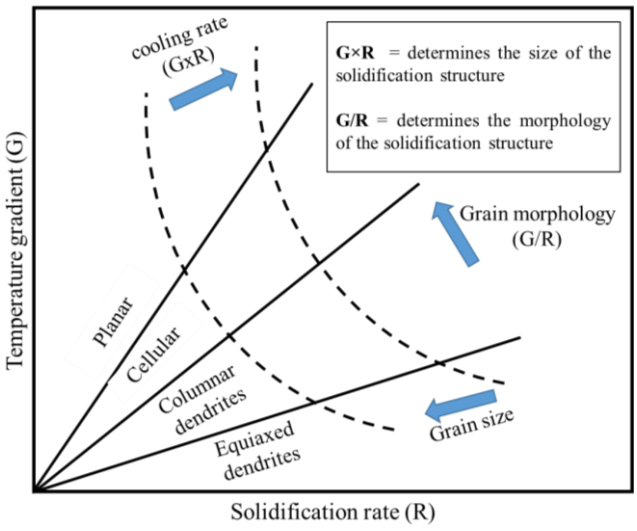

Fig 7. Schematic illustration of various solidification structures as a function of solidification rate (R) and temperature gradient (G) - adapted from [19].

In a previous study with tandem beam welding, it was observed that the introduction of a secondary beam flattens the temperature gradient along the transverse direction and reduces the mechanical restraint around the weld pool [20]. In our findings, at lower power ratios, the ring mode of the ARM beam is prominent in lowering the temperature gradient (and, potentially, the cooling rates) in the fusion zone due to the distribution of the beam over an enlarged area. As the power ratio increases, the temperature gradient produced in the fusion zone will increase due to the increase of power density by the core laser. A centreline crack-free window has been identified for *P*=5000 W and *P*=6000 W and discussed as follows:

- As the ring mode of the ARM beam is dominant at a lower power ratio of 0.36, partial bonding between the paltes with a reduced cooling rate and lower G/R were observed, therefore, coarse equiaxed and columnar grains are formed, as shown from the EBSD map in Fig. 6(b). Under these conditions, the coarse grains cannot withstand the transverse strains produced in the mushy zone, forming both transverse and centerline cracks.
- At a moderate power ratio of 1.5, a moderate sized equiaxed and columnar structure was facilitated by themoderate cooling rates and the stresses was distributed along with the increased number of grain boundaries in the fusion zone. Hence, low transverse strains were observed.
- When the power ratio further increased above 1.5, fine equiaxed grains were formed reduced the permeability of the dendritic network and facilitating the formation of transverse cracks, also the increased penetration depth with the power ratio and the columnar grains formed around the melt pool, redirects the mechanical restraints produced in the fusion zone and facilitating the formation of transverse cracks near the columnar grain boundaries. This result was also found in [21] and visible from the dye penetrant tests in Fig. 4(c).

To further confirm the results, the width specific number of grain boundaries near the top surface, "N", introduced by Hagenlocher et al. [22] is used: N is the ratio between the width of the equiaxed zone to the average equiaxed grain size. It indicates the number of grain boundaries in the weld zone, which can withstand the restraint produced during cracking. The higher the N value, the higher the reduction in crack susceptibility. From the EBSD maps, as shown in Fig. 6(b), it was observed that the N value was 28.56 at lower power ratios and increased to 40.8 at 1.5 and again decreased to 33.56 at higher power ratios, which supports our observation of crack formation as shown in Fig 6(a).

4. Conclusions

This paper studied the crack susceptibility of remote laser-welded AA 6005 alloy using different power ratios of the ARM co-axial beam. The main conclusions are:

- Although a linear dependency exists between the power ratio and the weld penetration depth, the same does not apply for the crack sensitivity - a parabola-like relationship was observed. Findings revealed that the cracking susceptibility is determined by the combined effect of the grain refinement (predominant at power ratios below 1.5) and the permeability in the fusion zone (predominant at power ratios above 1.5).
- A centreline crack-free window has been identified for P=5000 W and P=6000 W. As the power ratios increase to a threshold range of 1.5, the transverse strains are reduced, and no centreline cracks are observed. A high width specific equiaxed grain boundaries (N) were also observed near the power ratio of 1.5, which validates the DIC measurements.
- Further increasing the power ratios above 1.5 increases permeability and the mechanical restraints along the columnar grain boundaries and facilitate the formation of transverse cracks in the fusion zone. The width specific grain boundary value decreased at a higher power ratio of 2.5, which resulted in an increase in transverse strain and crack sensitivity.

Future work will be devoted to studying the effect of critical strain rate conditions using the DIC technique and understanding the strains which produce transverse micro-cracks in the joint at different grain morphologies of equiaxed and columnar grain structures. Furthermore, a combination of physical experiments and simulation will be sought to deepen

the understanding of the laser-material interaction with ARM laser technology.

Acknowledgements

This study was financially supported by (1) WMG HVM Catapult; (2) APC UK project: ALIVE - Aluminium Intensive Vehicle Enclosures; (3) Innovate UK IDP15 project LIBERATE: Lightweight Innovative Battery Enclosures using Recycled Aluminium Technologies; and (4) Innovate UK FASA: Flexible, Automated Stator Assembly.

References

[1] J. C. González Palencia, T. Furubayashi, and T. Nakata, "Energy use and CO2 emissions reduction potential in passenger car fleet using zero emission vehicles and lightweight materials," *Energy*, vol. 48, no. 1, pp. 548–565, 2012, doi: 10.1016/j.energy.2012.09.041.

[2] T. Sun, P. Franciosa, C. Liu, F. Pierro, and D. Ceglarek, "Effect of Micro Solidification Crack on Mechanical Performance of Remote Laser Welded AA6063-T6 Fillet Lap Joint in Automotive Battery Tray Construction," *Appl. Sci.*, vol. 11, no. 10, p. 4522, May 2021, doi: 10.3390/app11104522.

[3] W. Blendl and N. Cuppoletta, "Trend towards e-Mobility accelerates Aluminium Use," 2020. [Online]. Available: https://www.aluminium-messe.com/en/ALUMINIUM-2020/Trend-towards-e-Mobility-accelerates-Aluminium-Use/879/.

[4] M. Bloeck, "Aluminium Car Body Sheet : Alloys and Surface Pretreatments as System Solution Aluminium-Karosserieblech : Werkstoffe und Oberflächenvorbehandlungen als Systemlösung Average Use of Aluminium Per Car Western Europe," *Algr. Alusuisse*, pp. 1–32, 2001.

[5] S. Kou, *Welding Metallurgy*, Second ed. John Wiley & Sons, Inc., Hoboken, New Jersey, 2003.

[6] H. Wei, J. S. Chen, H.-P. Wang, and B. E. Carlson, "Thermomechanical numerical analysis of hot cracking during laser welding of 6XXX aluminum alloys," *J. Laser Appl.*, vol. 28, no. 2, p. 022405, 2016, doi: 10.2351/1.4944005.

[7] M. Rappaz, J. M. Drezet, and M. Gremaud, "A new hot-tearing criterion," *Metall. Mater. Trans. A Phys. Metall. Mater. Sci.*, vol. 30, no. 2, pp. 449–455, 1999, doi: 10.1007/s11661-999-0334-z.

[8] Z. Tang and F. Vollertsen, "Influence of grain refinement on hot cracking in laser welding of aluminum," *Weld. World*, vol. 58, no. 3, pp. 355–366, 2014, doi: 10.1007/s40194-014-0121-3.

[9] Z. Jiang *et al.*, "Grain refinement and laser energy distribution during laser oscillating welding of Invar alloy," *Mater. Des.*, vol. 186, p. 108195, 2020, doi: 10.1016/j.matdes.2019.108195.

[10] E. Arata, Yoshiaki; Nabegata, "Tandem Electron Beam Welding," *Osaka Univ. Knowl. Arch.*, vol. 7(1), pp. 101–109, [Online]. Available: http://hdl.handle.net/11094/6280.

[11] M. R. Maina, Y. Okamoto, A. Okada, M. Närhi, J. Kangastupa, and J. Vihinen, "High surface quality welding of aluminum using adjustable ring-mode fiber laser," *J. Mater. Process. Technol.*, vol. 258, no. March, pp. 180–188, 2018, doi: 10.1016/j.jmatprotec.2018.03.030.

[12] M. Sokolov, P. Franciosa, and D. Ceglarek, "Remote laser welding of die casting aluminum parts for automotive applications with beam oscillation and adjustable ring mode laser," *Laser Sytems Eur.*, vol. 44, no. 0, pp. 1–11, 2021, [Online]. Available: http://wrap.warwick.ac.uk/155751/.

[13] M. Kang, H. N. Han, and C. Kim, "Microstructure and solidification crack susceptibility of Al 6014 molten alloy subjected to a spatially oscillated laser beam," *Materials (Basel).*, vol. 11, no. 4, 2018, doi: 10.3390/MA11040648.

[14] D. Weller, C. Hagenlocher, T. Steeb, R. Weber, and T. Graf, "Self-restraint hot cracking test for aluminum alloys using digital image correlation," in *Procedia CIRP*, 2018, vol. 74, pp. 430–433, doi: 10.1016/j.procir.2018.08.165.

[15] N. Bakir, A. Gumenyuk, V. Pavlov, S. Volvenko, and M. Rethmeier, "In situ determination of the critical straining condition for solidification cracking during laser beam welding," *Procedia CIRP*, vol. 94, pp. 666–670, 2020, doi: 10.1016/j.procir.2020.09.104.

[16] E. J. Chun, K. Nishimoto, and K. Saida, "Evaluation of solidification cracking susceptibility in laser welds for type 316FR stainless steel," *Weld. World*, vol. 60, no. 2, pp. 217–231, Feb. 2016, doi: 10.1007/s40194-016-0293-0.

[17] C. Hagenlocher, P. Stritt, R. Weber, and T. Graf, "Strain signatures associated to the formation of hot cracks during laser beam welding of aluminum alloys," *Opt. Lasers Eng.*, vol. 100, pp. 131–140, Jan. 2018, doi: 10.1016/j.optlaseng.2017.08.007.

[18] J. Yang, "Finite Element Global Digital Image Correlation." MATLAB repository, 2021.

[19] W. Kurz and R. Trivedi, "Overview no. 87 Solidification microstructures: Recent developments and future directions," *Acta Metall. Mater.*, vol. 38, no. 1, pp. 1–17, 1990, doi: 10.1016/0956-7151(90)90129-5.

[20] J. Xie, "Dual beam laser welding," *Weld. J. (Miami, Fla)*, vol. 81, no. 10, pp. 223–230, 2002.

[21] B. Hu and I. M. Richardson, "Mechanism and possible solution for transverse solidification cracking in laser welding of high strength aluminium alloys," *Mater. Sci. Eng. A*, vol. 429, no. 1–2, pp. 287–294, 2006, doi: 10.1016/j.msea.2006.05.040.

[22] C. Hagenlocher, D. Weller, R. Weber, and T. Graf, "Reduction of the hot cracking susceptibility of laser beam welds in AlMgSi alloys by increasing the number of grain boundaries," *Sci. Technol. Weld. Join.*, vol. 24, no. 4, 2019, doi: 10.1080/13621718.2018.1534775.